ELSEVIER

Journal of Structural Geology 27 (2005) 913–928

JOURNAL OF STRUCTURAL GEOLOGY

www.elsevier.com/locate/jsg

Fault populations, strain distribution and basement fault reactivation in the East Pennines Coalfield, UK

W.R. Bailey[1], J.J. Walsh*, T. Manzocchi

Fault Analysis Group, Department of Geology, University College Dublin, Dublin 4, Ireland

Received 28 May 2003; received in revised form 6 February 2004; accepted 7 October 2004

Abstract

The scaling properties of faults within the East Pennine Coalfield (UK) are analysed for a fault population defined from a high quality, regional (ca. 1300 km^2) fault map for an Upper Carboniferous (Westphalian) coal seam. The fault system is dominated by an orthogonal network of NW- and NE-striking faults that preserve predominantly dip-slip extensional displacements ranging from <1 to 180 m. Fault displacements are post-depositional and late- to post-Carboniferous in age. Fault size (maximum throw, length and geometric moment) populations display very well defined power-law distributions over two orders of magnitude. Sub-sets of the population, discriminated in terms of sub-area (400 and 100 km^2) and strike (NW- and NE-striking sets) are also power-law distributed. Changes in the power-law exponents of NW- and NE-striking fault populations reflect strain variations across the area. Some sub-areas are dominated by NW-striking faults, whilst others display a more symmetrical fault pattern. This heterogeneous distribution of strain is strongly influenced by the geometry of an underlying lower Carboniferous (Dinantian) fault system, characterised by large NW-striking graben-bounding faults (km-scale throws), which localises strain in the upper Carboniferous cover sequence during late- and post-Carboniferous faulting.

Keywords: Fault populations; Fault reactivation; Strain localization

1. Introduction

High quality fault maps, containing a broad range of fault sizes, are a pre-requisite for the detailed analysis of the scaling properties of faults and fault systems. Such maps should, ideally, contain numerous faults (e.g. hundreds to thousands) with fault sizes (i.e. maximum throw, length, etc.) extending over several orders of magnitude and with displacement recorded along the lengths of individual fault traces. The spatial context of a fault map, and its fault population, should also be well defined so that account can be taken of a variety of sampling issues (e.g. censoring and truncation; see Pickering et al., 1994). These requirements are rarely, if ever, met by natural fault data sets, which usually provide a narrow range of well-defined fault sizes (<2 orders of magnitude), small numbers of faults (<100) and limited definition of fault displacements. Here we describe and analyse a 1300 km^2 high quality fault map derived from intensively mined coal seams within the Westphalian A–C fluvial/deltaic strata of the East Pennine Coalfield (EPC), UK (Fig. 1). The broad areal coverage, large number of faults ($n=7862$) and wide range of fault sizes (throws range from <1 to 180 m and lengths from 10 to 16 km) provides a basis for the rigorous analysis of fault population scaling properties. Our analysis concentrates on the scaling properties and spatial variations of fault length and maximum throw (i.e. vertical displacement) populations. We highlight the persistence of power-law scaling properties, which nevertheless show some spatial variations reflecting the geometry of underlying, and earlier, Dinantian normal fault systems.

* Corresponding author. Tel: +353 1 716 2169; fax: +353 1 716 2607
E-mail address: john@fag.ucd.ie (J.J. Walsh).
[1] Present address: CSIRO Petroleum, ARRC, 26 Dick Perry Avenue, Kensington, Perth, WA 6151, Australia.

0191-8141/$ - see front matter © 2005 Elsevier Ltd. All rights reserved.
doi:10.1016/j.jsg.2004.10.014

2. Regional context

The tectono-stratigraphic evolution of the EPC is best viewed in the context of the Variscan plate cycle defined by Fraser and Gawthorpe (1990) (Fig. 2), which comprises

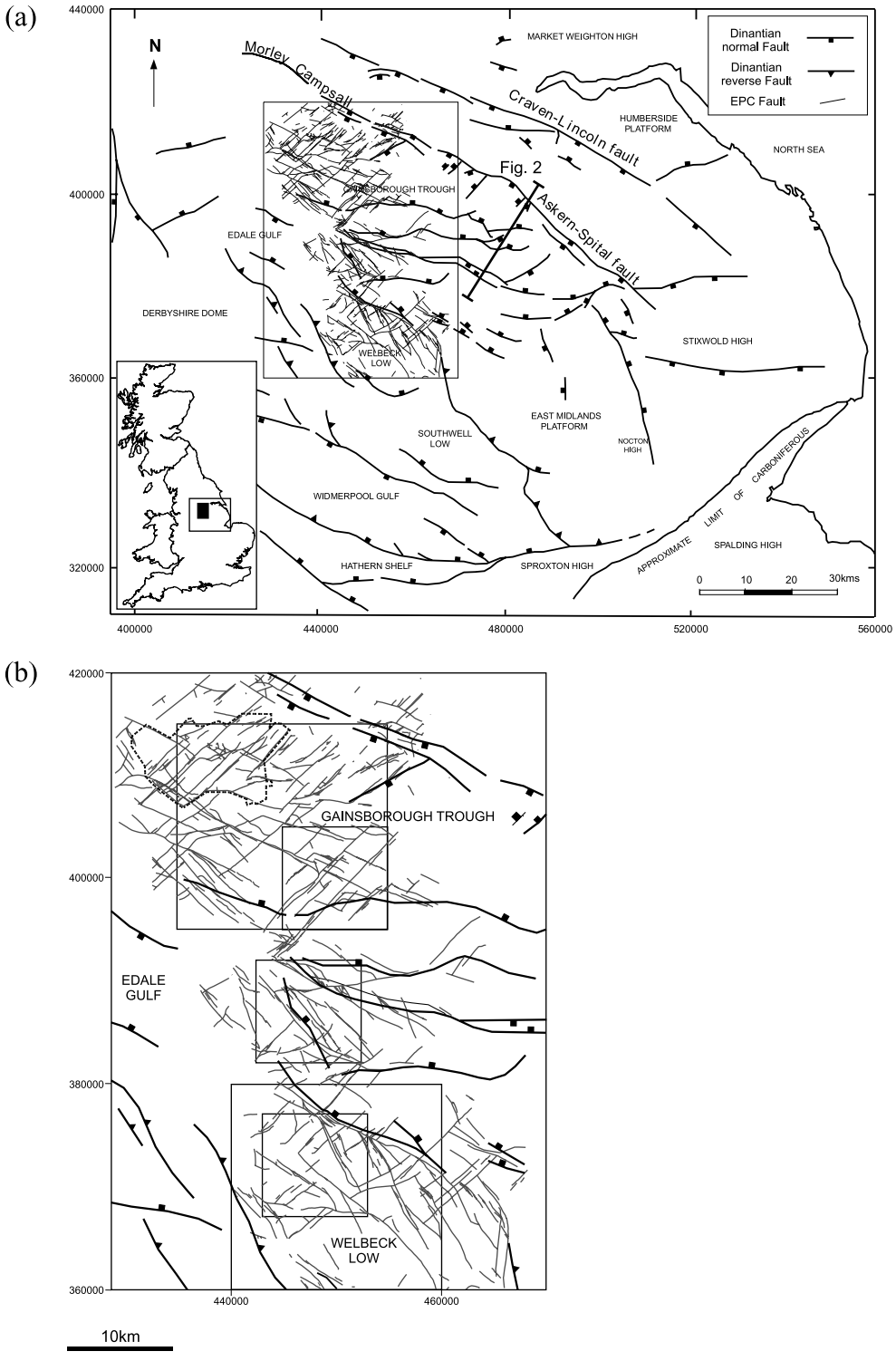

Fig. 1. (a) Map showing the location of the EPC study area with respect to the main structural elements in central mainland UK (inset). Faults in the EPC fault database with maximum throws greater than 5 m are shown (grey lines). Note the location of the cross-section shown in Fig. 2 (after Fraser and Gawthorpe, 1990). (b) Fault map for the Barnsley/Top Hard pseudoseam (grey lines) superimposed on the Dinantian fault map (black lines with tick marks), which is taken from Fraser and Gawthorpe (1990). For clarity, the EPC fault map only shows faults with maximum throws greater than 5 m. Note the coincidence between the location and orientation of Dinantian structures and the overlying EPC faults. The 20×20 km and 10×10 km sample areas used in this paper (black lines; Figs. 3 and 4), and the sample area in the north used by Watterson et al. (1996) (dashed), are shown.

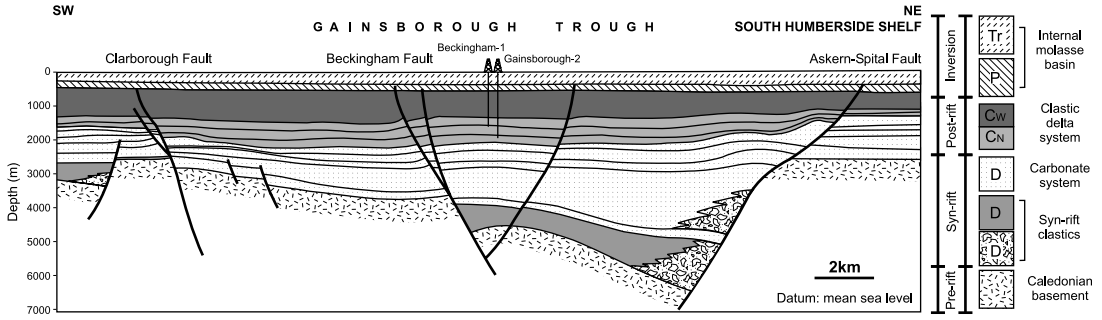

Fig. 2. Cross-section from the EPC showing the large-scale, syn-rift Dinantian structure, which underlies the Westphalian Coal Measures. D = Dinantian, C_N = Namurian, C_W = Westphalian, P = Permian, Tr = Triassic. Approximate line of section is shown in Fig. 1a: the map and section are modified from Fraser and Gawthorpe (1990, 2003) and not all the faults observed on the section are shown on the map.

syn-rift, post-rift and inversion tectonic phases dating from late Devonian to early Permian times. This basic tectono-stratigraphic framework has been defined using both borehole and seismic data arising from hydrocarbon exploration and production in the Carboniferous of northern England. Hydrocarbon accumulations are sited within Dinantian, Namurian and lower Westphalian reservoirs, stratigraphically underlying the coal seams from which the EPC fault map was generated. Approximately N–S extension during Dinantian rifting saw the development of major half-grabens bounded by WNW- to NW- and, to a lesser extent, NE-striking faults with up to km-scale displacements (Figs. 1 and 2; Fraser and Gawthorpe, 1990). The resultant regional Dinantian architecture is dominated by major WNW- to NW-trending fault systems and asymmetric grabens, which include the Gainsborough and Widmerpool basins (Fig. 1; Fraser and Gawthorpe, 1990; Rippon, 1997). This rifting gave way to mainly tectonically passive, thermally-driven, subsidence in the Namurian and Westphalian, during which the East Pennine Coal Measures were deposited in a fluvial–deltaic environment (Fraser and Gawthorpe, 1990). Evidence of minor fault reactivation and syn-depositional displacements during the Namurian–Westphalian A interval is recorded on only the largest faults (e.g. Askern Spital and Morley–Campsall faults; Figs. 1 and 2). This fault activity ceased during late Westphalian A to Westphalian C times when the Coal Measures were deposited. The transition from thermal subsidence to Variscan inversion tectonism is marked by the formation of the normal fault systems seen within the Coal Measure sequences of the EPC. The tectonic significance of these faults is as yet unclear, though they appear to be a response to approximately N–S extension, immediately preceding the onset of Variscan shortening, and possibly synchronous with compression further to the south (Woodcock and Strachan, 2000). Seismic data indicate that the larger of these normal faults are sometimes caused by minor reactivation (i.e. <150 m displacement) of major, km-scale displacement, Dinantian normal faults (Fig. 2). In the EPC, later relatively weak N–S Variscan compression is accommodated by the generation of occasional gentle folds, sometimes as inversion anticlines within the hanging walls of large faults, and by the strike-slip reactivation of WNW–NW-striking faults (Fig. 1; Rippon, 1997). Evidence of inversion of fault displacements, to provide reverse faults, is very rare and only observed on seismic sections, but where present is associated with the generation of tight hanging wall anticlines that sometimes provide closure to hydrocarbon reservoirs (Fraser and Gawthorpe, 1990). Variscan shortening is responsible for the uplift and erosion of syn- and post-rift Carboniferous sediments, prior to the deposition of sediments above a regional-scale Permian unconformity. Sub-ordinate amounts of extensional reactivation, typically representing less than 20% of the total displacement, has occurred on some normal faults in post-Permian unconformity times; the origin and precise timing of these displacements is unknown.

3. EPC structure

The present day regional bed dips within the Coalfield are on average 3–4° E, but locally high dips are associated with normal fault-related folding (i.e. drag) or with later Variscan inversion folds (Goossens and Smith, 1973; Gibson et al., 1989). Coalfield faulting is predominantly extensional and of late-Westphalian to pre-Permian in age. Faulting is post-coalification/lithification and is believed to have taken place close to the maximum burial depth of the Coal Measures (Rippon, 1985a,b; Walsh and Watterson, 1988a, 1989), prior to compression-related uplift and erosion. However, in parts of the Coalfield up to 25%, but more generally $<10\%$, of the displacement on the largest faults (i.e. those faults with maximum throws >100 m) post-dates the deposition of the unconformably overlying Permian succession (Elliott, 1954 (National Coalboard Report); Watterson et al., 1996). Based on interpretation of regional 2-D seismic reflection lines and depositional patterns, occasional large faults (e.g. >100 m throw; Morley–Campsell Fault: Fig. 1) display evidence of pre-Westphalian syn-depositional displacements (Fraser and Gawthorpe, 1990; Rippon, 1997). Compactional and

gravity-slide syn-depositional faults, which are vertically (i.e. <50 m) and laterally less persistent than tectonic faults, are present within the Coal Measures. However, these structures are easily distinguished from tectonic faults since they display arcuate traces in map view and are abundant at certain stratigraphic levels (e.g. Blackshale seam). These non-tectonic syn-depositional faults are not incorporated in the database.

Tectonic faulting in the EPC is dominated by an orthogonal network of NW-striking (including WNW–NW strikes) and NE-striking normal faults with throws up to ca. 200 m (see also Graham, 1988; Watterson et al., 1996). Faults with both strike directions dip east and west in approximately equal amounts. Significantly, the locations and geometries of a number of major NW-striking faults in the Coal Measures are coincident with the larger Dinantian normal faults at depth (Fig. 1). No clear consistent cross-cutting relationships of faults are observed in the Coal Measures, which suggests that the NW- and NE-striking normal faults are contemporaneous (Watterson et al., 1996). However, a number of WNW-striking fault zones in the EPC dextrally offset and, therefore, at least partly post-date the normal faults, which sometimes show more subtle indications of a component of strike-slip displacement (i.e. oversteepening of fault surfaces, switching of dip-slip sense of displacement). Examples include the Inkersall fault zone in Derbyshire and the Holgate Hospital and North Gawber fault zones in South Yorkshire, which parallel the major, 4-km-wide Morley–Campsall strike-slip fault zone in the far north of the map area (Figs. 1 and 3). These zones are characterised by relatively high fault density and, although they can record large (>100 m maximum) normal displacements, they also display strike-slip offsets, which, for the Holgate Hospital fault zone, may be >300 m dextral (Goossens and Smith, 1973; Watterson et al., 1996; Fig. 3). These strike-slip displacements are attributed to late Carboniferous deformation and are consistent with approximately N–S directed Variscan regional shortening and related dextral shear on the eastern side of the Pennines Block (Woodcock and Strachan, 2000), and with the formation of NW-trending folds, such as the Brimington Anticline (Figs. 1 and 3; Goossens and Smith, 1973; Fraser and Gawthorpe, 1990; Rippon, 1997). Variscan shortening may also be responsible for the rare examples of reversal of original normal fault displacements seen on seismic data (Fraser and Gawthorpe, 1990) from the southern part of northern England, either well outside of, or bounding, the EPC fault map area (Fig. 1b); there is no evidence from mine data that such reversed displacements occur at the mapped stratigraphic level within the EPC fault map.

4. The fault database

The EPC fault map and database are underpinned by high quality and high density coal seam extraction mine plan data, which have been manually digitised. The ca. 1300 km^2 mapped area has been mined so extensively, not just areally but also vertically, by multi-seam workings that near complete areal coverage is attained by combining data from a number of seams. The EPC fault map is based on the regionally correlatable seam colloquially referred to as the Top Hard (Staffordshire/Derbyshire/Nottinghamshire) or Barnsley (Yorkshire). Deep coal mine plan data for multi-seam workings (all within a ca. 150-m-thick sequence) have been combined to provide almost complete areal coverage for what is referred to as a 'pseudoseam' map of the Top Hard/Barnsley seam (Fig. 3). The following is a brief description of the raw data and method of fault map construction; further details are given in Watterson et al. (1996).

4.1. Raw data and database construction

For most of the 1900s, seam abandonment plans were generally produced on 2×1 km sheets at a scale of 1:2500. The raw data recorded on the mine plans are the boundaries of the workings, seam elevations in the form of 'spot heights' and contours, fault traces and throw values recorded, on average, every ca. 100 m along each fault trace. Given the preponderance of normal faults within the EPC (Graham, 1988; Walsh and Watterson, 1988a; Watterson et al., 1996), fault throw represents a good measure of fault displacement; strike-slip faults are identified from fault geometry attributes, such as reversals of fault dip and throw direction or, less often, lateral offsets of earlier faults. The minimum throw values recorded are typically ca. 8 cm (or 3 inches), but more commonly 15 cm (or 6 inches). Throws greater than ca. 3 m (i.e. significantly greater than the <1 m thick coal seams) are calculated from the offset of seam elevations derived from levelling data, whilst throws of less than ca. 3 m are generally measured by mine surveyors and recorded directly on coal seam plans. The quality and extent of the data varies with the age of workings. The highest quality data are derived from post-1950s workings, whilst the most areally complete plans are of pre-1970s age. The final pseudo-seam map includes the highest quality data available for different parts of the map area.

The aim of the database was to combine fault and seam elevation data from a number of seams to generate the most extensive areal coverage possible. The most intensively and extensively worked seam throughout the Coalfield is the regionally correlated Top Hard/Barnsley, which is located in the upper–middle part of the Coal Measures. All fault and seam elevation data for this seam were digitised and used to build the fault map. Where abandonment plans are not available for this seam or where the quality of fault and fault displacement data were suspect (i.e. particularly for older workings), data gaps were removed either by lateral extrapolation and interpolation (see Walsh and Watterson (1990) for methods) and/or by using data from the vertically

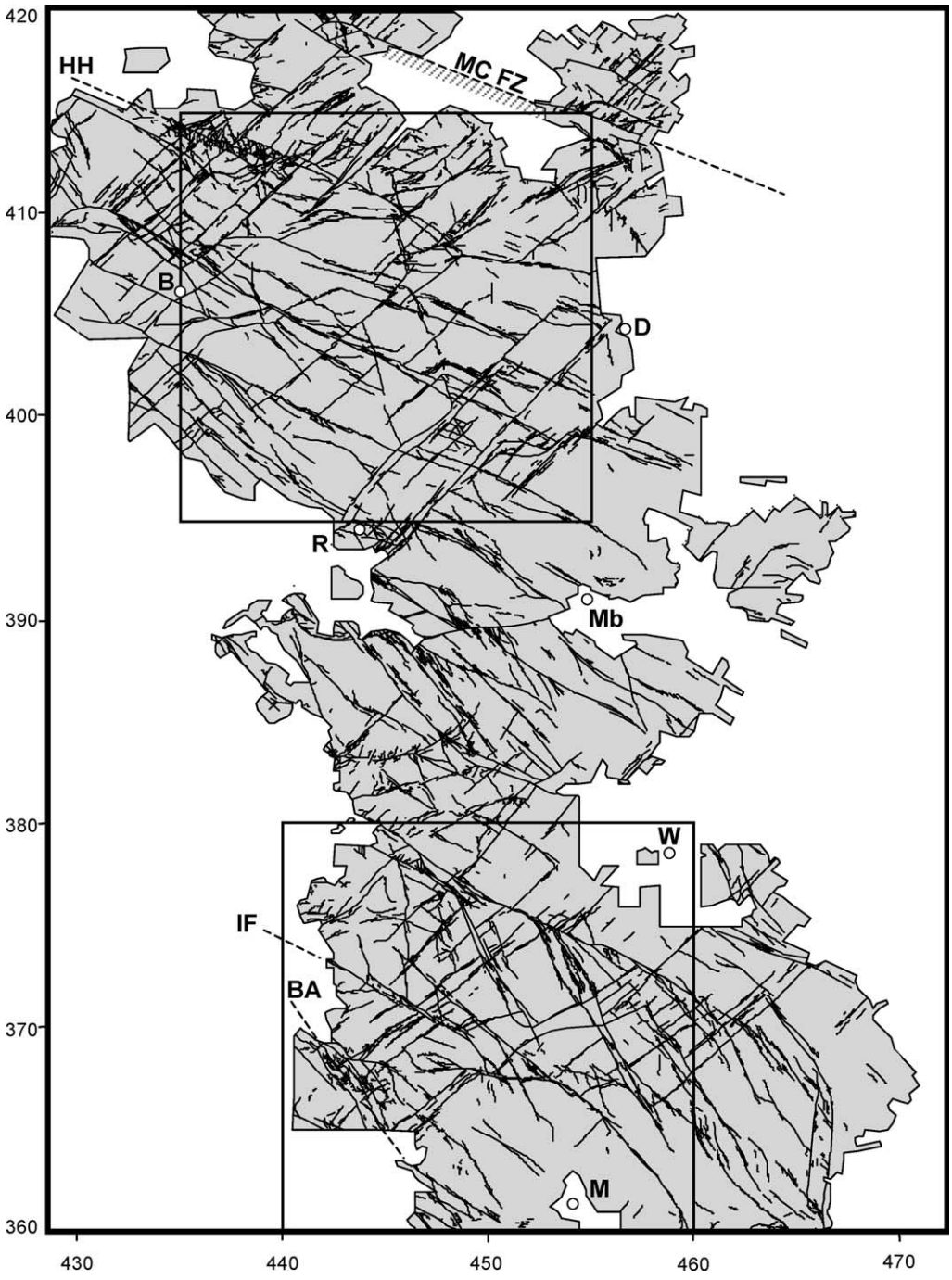

Fig. 3. Fault map for the Barnsley/Top Hard pseudoseam showing all faults within the database with maximum throws greater than 1 m. Shading shows the extent of the mined area included in the map. The names and locations of towns and major structures referred to in the text are shown: B, Barnsley; BA, Brimington Anticline; IF, Inkersall Fault Zone; D, Doncaster; HH, Holgate Hospital Fault Zone; M, Mansfield; Mb, Maltby; MCFZ, Morley–Campsall Fault Zone; R, Rotherham; W, Wakefield.

nearest, best quality seam plan. The method of extrapolating data from vertically disposed seams is justified by the vertical persistence of the faults, which suggests that faults on one seam are expected on vertically adjacent seams. For example, the smaller faults in the Coalfield with 1 m throws are known to extend more than 100 m up- and down-dip on the basis of contoured displacement patterns and measured vertical throw gradients (Rippon, 1985a,b; Walsh and Watterson, 1989). The combination of data from different seams generates a small lateral shift of the fault traces of the same fault on adjacent seams. This effect arises from the dips of faults, and is not significant on the scale of the study area.

Fault and seam elevation data from the abandonment

plans have been digitised using a conventional mapping package. Boundaries of workings, seam elevations and fault trace and throw data are recorded. Fault traces are recorded in centre-line format with associated throw values and throw directions. The type of fault terminations are also recorded, e.g. tips, end of data or abutment. The final digitised data form a single 'pseudoseam' map for the Top Hard/Barnsley seam, which represents the highest quality data over the largest area possible (Fig. 3). The map covers an area of ca. 1300 km^2 and contains 7862 faults and over 31,000 throw values. On average there is one throw reading per ca. 100 m of fault trace. A total of 6332 faults have maximum throws greater than 0.91 m (3 ft), 1248 have smaller maximum throws and 282 faults have no recorded throw values; these faults have trace lengths less than 200 m and are therefore unlikely to have maximum throws greater than ca. 50 cm. Although some faults with maximum throws smaller than 0.9 m are included in the database, many more appear on the abandonment plans but have not been digitised since the resolution of the dataset is a function of the poorest quality mine-plans, and on these plans only faults larger than 3 ft are recorded. In areas with higher resolution mine plans (e.g. South Yorkshire; Watterson et al., 1996) inclusion of all mapped faults would increase the size of the dataset by more than a factor of four.

5. Fault analysis

Fault patterns vary considerably across the EPC map (Figs. 1 and 3). The fault system in the south is dominated by two main through-going, WNW-striking faults, which are linked by numerous NE- and NNW-striking faults (Figs. 1b, 3 and 4a). WNW–NNW-striking faults are even more dominant in the central part of the map, whereas the majority of the northern part of the fault map is characterised by a more symmetrical, orthogonal network of WNW- and NE-striking faults (Figs. 1b, 3 and 4b). This variability appears to be related to the distribution of underlying major Dinantian normal faults, which have previously been mapped from regional 2-D seismic data (Fig. 1a; Fraser and Gawthorpe, 1990). For example, the central and southern parts of the fault map overlie relatively closely spaced NW- to W-striking Dinantian faults (Fig. 1). The northern area, by contrast, overlies the ca. 20-km-wide Gainsborough Trough which is relatively unfaulted. In the following sections we determine population systematics for the whole EPC and for sub-sets of the whole population discriminated in terms of area and strike. The principal purposes are to establish the scaling properties of fault size distributions and to examine the extent to which these can be related to differences in the underlying Dinantian structure.

5.1. Displacement–length relationships

Each fault in the database has a length and maximum throw, which allows quantitative assessment of the fault size population. Previous work has shown that there is a systematic relationship between the maximum displacement (D) and length (L) of faults, such that:

$$D = cL^n$$

where c is a constant relating to material properties and the exponent n typically ranges from 1 to 2 for tectonic fault systems (e.g. Ranalli, 1977; Watterson, 1986; Walsh and Watterson, 1988b; Marret and Allmendinger, 1991; Cowie and Scholz, 1992a; Dawers et al., 1993); n values, however, have been noted for scale-bound fault systems at low strains (e.g. Ackermann et al., 2001; Schultz and Fossen, 2002). Although this scaling relationship underpins simplistic models of fault growth, natural datasets display large variations in displacement:length ratios (e.g. Walsh and Watterson, 1988b; Marret and Allmendinger, 1991; Cowie and Scholz, 1992b; Gillespie et al., 1992), which may be attributed to measuremental error, lithological variations, fault interaction and strain (e.g. Wojtal, 1994; Cartwright et al., 1995; Dawers and Anders, 1995; Poulimenos, 2000; Walsh et al., 2002). These complicating factors, combined with the rather limited size range (i.e. 1–2 orders of magnitude) of most natural datasets, make an accurate determination of n inherently problematic. The very high quality of the EPC fault map is, however, exceptional and the derived displacement–length relationship, in which $n \sim 1.22$ (derived from Reduced Major Axis regression), is not subject to some of the sampling and data quality limitations inherent in other datasets (Fig. 5). Several geological issues are not, however, accounted for in this relationship. Fig. 5 contains all EPC data, which includes cross-cutting faults and fault segments bounding relay zones, i.e. the full range of hard- to soft-linkage (Walsh and Watterson, 1991). Nevertheless even if only tip-to-tip faults are considered (Gillespie et al., 1992), a very similar n value of ~ 1.19 is derived (Fig. 5).

5.2. Fault populations

Numerous studies have demonstrated that fault size populations follow power-law distributions, such that:

$$N \propto S^{-C_s}$$

where N is the number of faults of size greater than or equal to S and C_S is the power-law exponent (e.g. Kakimi, 1980; Walsh and Watterson, 1988b; Childs et al., 1990; Heffer and Bevan, 1990; Jackson and Sanderson, 1992; Pickering et al., 1994). On a plot of $\log N$ against $\log S$, a power-law distribution is defined by a straight line segment with slope $-C_S$. The most commonly used measures of fault size for fault map data are the fault trace length, hereafter referred to as fault length, and the maximum displacement, which for faults derived from coal mine data is taken as the maximum throw. Here we examine the characteristics of the fault length, maximum throw and geometric moment populations of the EPC fault map.

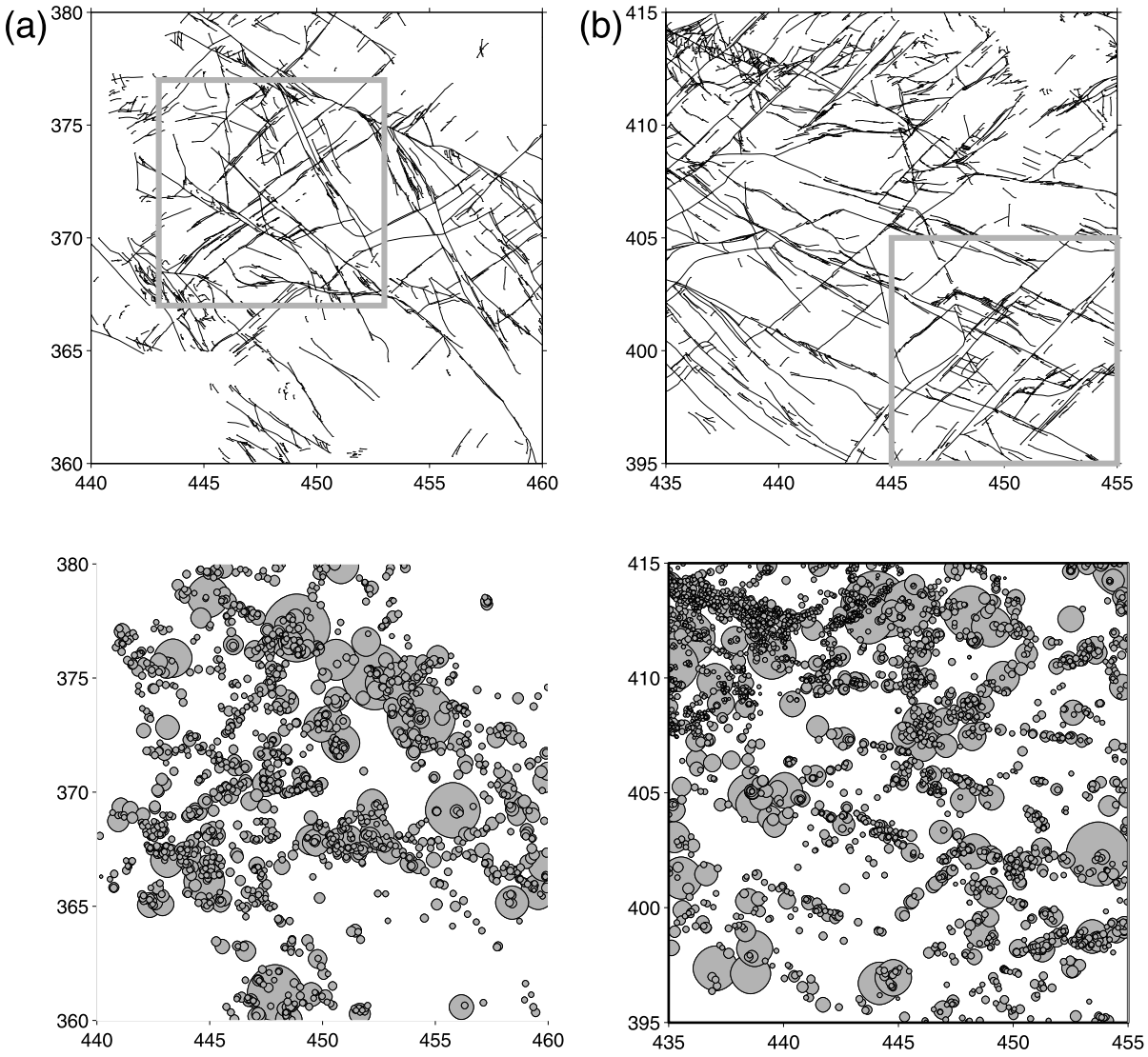

Fig. 4. Fault maps (top) and positions of maximum fault throw for individual fault traces (bottom) in the 20×20 km and 10×10 km (grey boxes) sample areas. Circle areas are proportional to throw and are at the positions of maximum throw of individual faults: (a) southern area (maximum throw = 142 m), and (b) northern area (maximum throw = 180 m). For positions of sample areas see Figs. 1a and 3.

The maximum throw population for all faults within the EPC shows a power-law distribution over two orders of magnitude (Fig. 6a). The lower size limit of 0.91 m was imposed during digitisation of the raw fault data and is therefore a *truncation* effect (Heffer and Bevan, 1990; Jackson and Sanderson, 1992). The drop off at the high displacement end of the population curve, which occurs at approximately 100 m, would generally be attributed to *censoring* effects. However, the very large areal extent of the EPC fault map (1300 km^2) combined with constraints from areas outside the EPC study area suggests that this limit is a fundamental property of the scaling of this fault system; this issue is returned to later. The straight central segment of the population curve between 1 and 100 m yields a value of C_D of 1.22 ($R^2 = 0.997$) and is comparable with those determined from a variety of tectonic fault systems, which range from ca. 1.0 to 1.5 (e.g. Scholz and Cowie, 1990; Marret and Allmendinger, 1992; Gauthier and Lake, 1993; Villemin et al., 1995; Watterson et al., 1996; Yielding et al., 1996). Despite the excellent power-law fit ($R^2 = 0.997$) for this central segment, there is some indication that the population curve slightly steepens towards lower throw values, the possible significance of which is returned to later.

The fault length population for the whole EPC provides a gently curved distribution (Fig. 6b). Previous work has shown that non power-law fault length distributions can arise from sampling effects, the most important of which is the difficulty of defining the positions of fault tips which, by definition, are associated with displacements below the displacement resolution of the dataset (Watterson et al., 1996; Yielding et al., 1996). These deficiencies can be

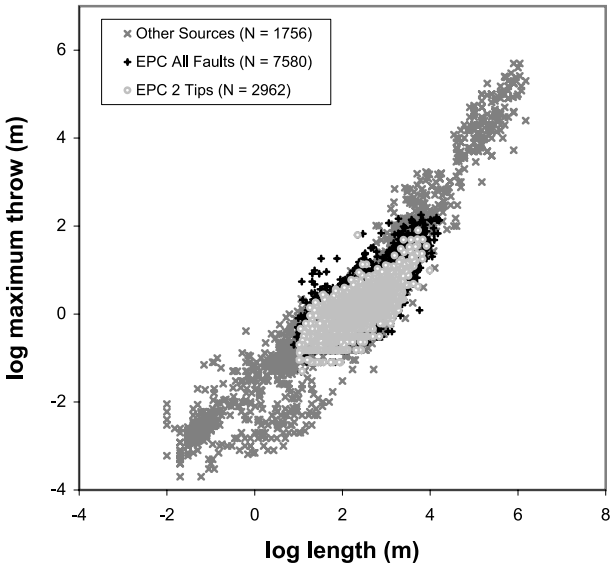

Fig. 5. Throw vs. length data for the entire EPC (black crosses) and for only those faults with two fault tips (grey circles) plotted over data derived from numerous published sources (grey crosses; Beck, 1929; Reeves, 1929; Teas, 1929; Babenroth and Strahler, 1945; Fox, 1959; Brunstrom, 1963; Woodland and Evans, 1964; Tschop, 1967; Janoschek and Götzinger, 1969; Wood et al., 1969; Freund, 1970; Mayuga, 1970; Bond et al., 1971; MFRG, 1973; Huntoon, 1974; MacMillan, 1975; Elliott, 1976; Cave, 1977; Ruzhich, 1977; Shepherd and Burns, 1978; Frost and Smart, 1979; Drozdzewski et al., 1980, 1985; Frost and Halliday, 1980; Nelson, 1980; Verdier et al., 1980; Van den Bark and Thomas, 1981; Muraoka and Kamata, 1983; Aitkenhead et al., 1985; Villemin and Sunwoo, 1987; Opheim and Gudmundsson, 1989; Walsh and Watterson, 1988b; Gillespie, 1991; Marret and Allmendinger, 1991; Peacock, 1991; Gillespie et al., 1992; 1993 and references therein; Dawers et al., 1993; Davison, 1994; Dawers and Anders, 1995; Cartwright et al., 1996; Jackson et al., 1996; Nicol et al., 1996; Schlische et al., 1996; Rowan, 1997; Fossen and Hesthammer, 1998).

addressed in a number of ways, the most direct being to estimate the extent to which faults are likely to be shortened by this sampling effect. Examination of coal mine plans, complemented by constraints from fault population curves, show that faults with maximum throws below ca. 50 cm are under-represented in mine plan data and that fault throws less than 10 cm are very rarely recorded (see also Watterson et al., 1996). The limit of resolution for fault throws (i.e. the throw value below which fault traces will not be mapped) therefore lies somewhere between 10 and 50 cm. Previous work has shown that coalfield faults are characterised by horizontal displacement gradients generally within the range of 0.01–0.001, values that are consistent with the range of maximum throw/length ratios of faults in the EPC (the ratio of D/L for those faults with two tips is approximately log-normally distributed with a mean value of log (D/L) of -2.23 i.e. 0.006). Combining the variability in both horizontal displacement gradients and throw resolution suggests that trace length increases of between 60 and 150 m per fault tip (i.e. 120–300 m per fault trace) are required to account for errors associated with fault tip resolution. Introducing these corrections has a dramatic

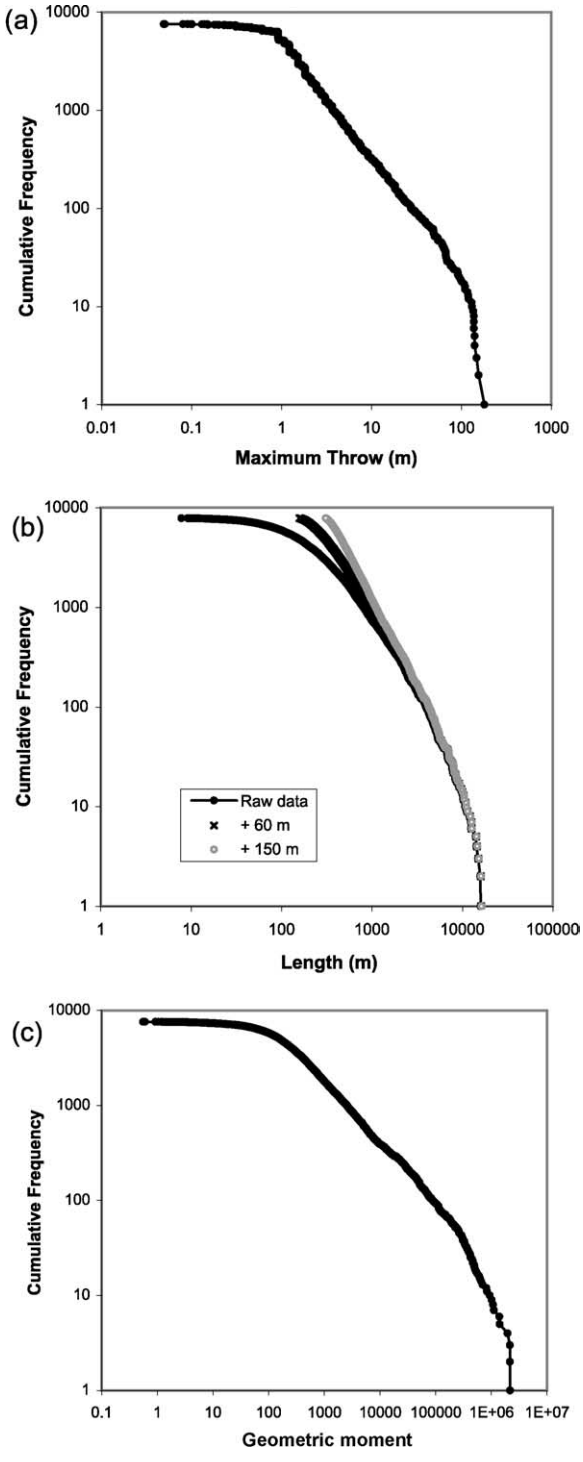

Fig. 6. Fault size populations for the entire EPC. (a) Maximum throw, (b) fault trace length, and (c) geometric moment. (a) Maximum throw population showing a straight-line power-law distribution with a slope of -1.22 from 0.91 m to ca. 150 m ($N=7580$). (b) Raw fault trace length population (black; $N=7862$) showing a gently curved distribution, which is due to the poor resolution of faults using mine plan data, particularly at the low displacement ends of faults towards their tips. This effect is corrected by adding 60 m (black crosses) and 150 m (grey circles) to the fault tips, which results in population curves that are approximately power-law with exponents between 1.37 and 1.72 (see text for discussion). (c) Geometric moment (length × average throw) population ($N=7580$).

effect on the fault length population curves, with the emergence of well-defined power-law distributions with C_L between −1.4 and −1.75, values that are within the range previously determined from tectonic fault datasets (−1.0 to −1.7: Gauthier and Lake, 1993; Scholz et al., 1993; Villemin et al., 1995; Watterson et al., 1996). Using the relationship $C_L/C_D=n$, where C_L and C_D are power law exponents for length and maximum throw distributions, respectively, provides an estimate of n of between 1.15 and 1.43 (Watterson et al., 1996), values which are consistent with those established from D vs. L plots for the entire dataset (1.22) and for tip–tip faults that have been tip-corrected.

Cumulative frequency plots of geometric moment, which is the product of the fault length and average throw (Marret and Allmendinger, 1990), allow an assessment of the scaling properties of strain (Fig. 6c). The strain associated with normal fault systems is a function of the geometric moment, such that for a given fault dip the extensional strain within an area is proportional to the ratio of geometric moment to area; our strain estimates assume an average fault dip of 69°, a value derived from 3131 dip measurements on 110 faults from the EPC by Walsh and Watterson (1988a), and do not account for any later strike-slip deformations. The geometric moment population has a shallower slope, of ca. 0.61, than either the maximum throw or fault length populations, reflecting both the positive correlation between these parameters and the disproportionate accommodation of regional strain on the largest faults. For example, 90% of the strain is accommodated on no more than 12% of the faults (approximating to all the faults with maximum throws greater than 6.5 m), and 60% of the strain is accommodated by the largest 1% of the faults (approximating to those faults with maximum throws greater than 45 m). The contribution of faults smaller than the resolution of the data can be estimated by extrapolating the population down to geometric moments of zero: this increases the total strain by less than 0.3%. These results highlight the heterogeneous distribution of strain in the EPC fault system, a feature we explore further in the next section.

5.2.1. Sub-areas

Spatial variations in the fault populations and therefore the strain distributions of the EPC fault system are examined by comparing the fault size populations from the whole EPC with those of smaller (20×20 km and 10×10 km) sub-areas. Our analysis concentrates on comparing the contributions of different fault sets (i.e. strikes) to the maximum fault throw population of the entire area. A more rigorous analysis of the spatial variations in the scaling properties of the fault population is beyond the scope of this paper and is the focus of ongoing work.

The EPC fault system has been subdivided into three principal sub-areas: southern, central and northern (Figs. 1, 3 and 4). These sub-areas are characterised by different fault patterns, with a rather symmetrical pattern of WNW- and NE-striking faults developed in the north, giving way southwards to the WNW- and NNW-striking faults of the central sub-area, a pattern that is further complicated by the inclusion of a greater number of NE-striking faults in the southern area. Despite these spatial variations in fault patterns, maximum throw (Fig. 7) and length (not shown) population curves derived from 20×20 km and 10×10 km sub-areas across the EPC fault system yield power-law populations with broadly similar exponents that are comparable with those for the whole population. The maximum throw populations display relatively consistent curves with the power-law exponent ranging from 1.19 (north 10×10 km sample) to 1.24 (south 10×10 km sample) with only the southern 20×20 km area providing a slightly higher value of 1.35 (Fig. 7; Table 1). Watterson et al. (1996) derived a C_D of 1.14±0.07 for their 87 km^2 study in the north (see Fig. 1b for location), which compares well with the 1.21 and 1.19 obtained here for the 20×20 and 10×10 km northern areas, respectively (Table 1). Since the southern 20×20 km area is characterised by the lowest measured strain (0.0107 as opposed to the 0.0161–0.0207 range for other areas), it would appear that the strain accommodated by a fault system may be inversely related to population exponent, a suggestion that is explored further in the next section.

5.2.2. NW- and NE-striking fault sets

In order to quantify the contribution that faults of different strikes make to the whole fault system, the fault size populations are sub-sampled into NW- (WNW–NNW) and NE-striking sets. For the whole EPC (Fig. 8) the slopes for the maximum throw populations are shallower for the NE-striking faults ($n=3241$) than the more abundant NW-striking faults ($n=4336$); $C_D=1.16$ and 1.27, respectively. The sum of the geometric moments for the NW- and

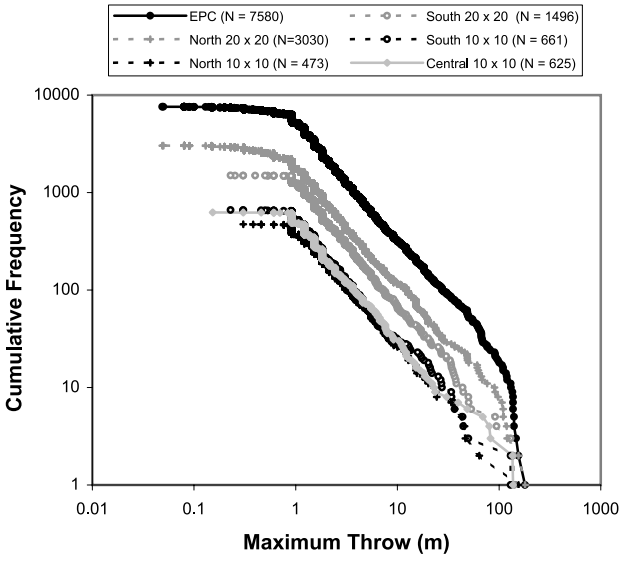

Fig. 7. Maximum throw populations for the entire EPC and for all of the sub-areas discussed in the text.

Table 1
Population slopes derived from maximum throw distributions. 'Sum moment' is the sum of the geometric moments (i.e. the product of fault length and average throw) for all faults in the sample area. Strain is the extensional strain (i.e. fault heave per unit area) which, assuming a fault dip of 69°, is calculated by dividing 'sum moment'/area by tan 69°. The two percentage columns on the right-hand side refer to the percentage strain accommodated on, and percentage number of, NW- and NE-striking faults within a sample area

Area	Strike	Number of faults	Population slope (C_D)	Area (km^2)	Sum moment	Strain	Strike	
							% Strain	% Number of faults
All EPC	Both	7580	1.22	1323	5.43×10^7	0.0157	–	–
North 20×20	Both	3030	1.21	400	1.78×10^7	0.0169	–	–
North 10×10	Both	473	1.19	100	4.25×10^6	0.0161	–	–
Central 10×10	Both	625	1.22	100	5.37×10^6	0.0207	–	–
South 20×20	Both	1496	1.35	400	1.11×10^7	0.0107	–	–
South 10×10	Both	661	1.24	100	5.09×10^6	0.0196	–	–
All EPC	NW	4336	1.27	1323	2.91×10^7	0.0084	53.56	57.23
All EPC	NE	3241	1.16	1323	2.52×10^7	0.0073	46.44	42.77
North 20×20	NW	1616	1.33	400	5.36×10^6	0.0050	30.14	53.33
North 20×20	NE	1414	1.10	400	1.24×10^7	0.0119	69.86	46.67
North 10×10	NW	266	1.30	100	6.37×10^5	0.0023	14.99	56.24
North 10×10	NE	207	1.05	100	3.61×10^6	0.0138	85.01	43.76
Central 10×10	NW	485	1.23	100	3.80×10^6	0.0146	70.76	77.85
Central 10×10	NE	138	1.12	100	1.57×10^6	0.00061	29.24	22.15
South 20×20	NW	913	1.22	400	9.17×10^6	0.0088	82.51	61.03
South 20×20	NE	583	1.35	400	1.94×10^6	0.0019	17.49	38.97
South 10×10	NW	372	1.16	100	4.01×10^6	0.0154	78.70	56.28
South 10×10	NE	289	1.34	100	1.08×10^6	0.0042	21.30	43.72

NE-striking fault sets are 2.9×10^7 and 2.5×10^7 m^2, respectively, which indicates that the more numerous NW-striking faults are slightly more important in terms of accommodating regional strain despite the largest faults striking NE. Such complexities at the scale of the whole EPC are attributed to the heterogeneous distribution of strain and are best addressed by analysis of smaller areas.

Figs. 9–11 show maximum throw populations for the southern, central and northern sub-areas sub-sampled by strike. In the southern sub-areas, NW-striking faults accommodate the bulk of the strain, are larger and more abundant than the NE set and also display lower population slopes (Fig. 9). By contrast in the northern sub-areas, NE-striking faults dominate the strain, are larger and have lower population slopes (Fig. 11) than NW-striking faults. The central 10×10 km sub-area, although dominated by NW-striking faults, both in terms of strain and number of faults, provides a slightly lower slope for NE-striking faults (Fig. 10). The nature of these changes in strain and population slope can be explored further by reference to a study of a number of normal fault systems by Moriya et al. (2005). Their study demonstrates an inverse correlation between the strain accommodated on the individual dip-populations and their population slopes (Fig. 12). The principal conclusion to be drawn from this relationship is that an increase in strain is accompanied by a greater proportion of that strain being accommodated on larger faults, to provide a more localised fault system with continued fault system growth (Cowie et al., 1995; Ackermann et al., 2001; Moriya et al., 2005). Despite the reversal of the dominant fault orientation between the northern and southern areas in the EPC, the relatively low-strain EPC data fall near the centre of the trend of slope against strain observed in other normal fault systems (Fig. 12) and the EPC strike-population slopes also define a weak inverse correlation with strain. These relationships are consistent with the notion that higher strain fault sets within the EPC are generally characterised by lower population slopes and are, as a consequence, better localised than lower strain fault sets; the origin of this localisation is discussed further in the next section.

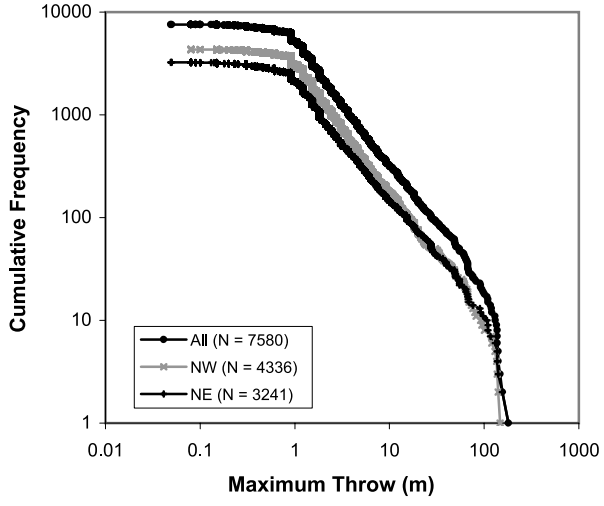

Fig. 8. Maximum throw populations for the entire EPC and for NW- and NE-striking fault sets.

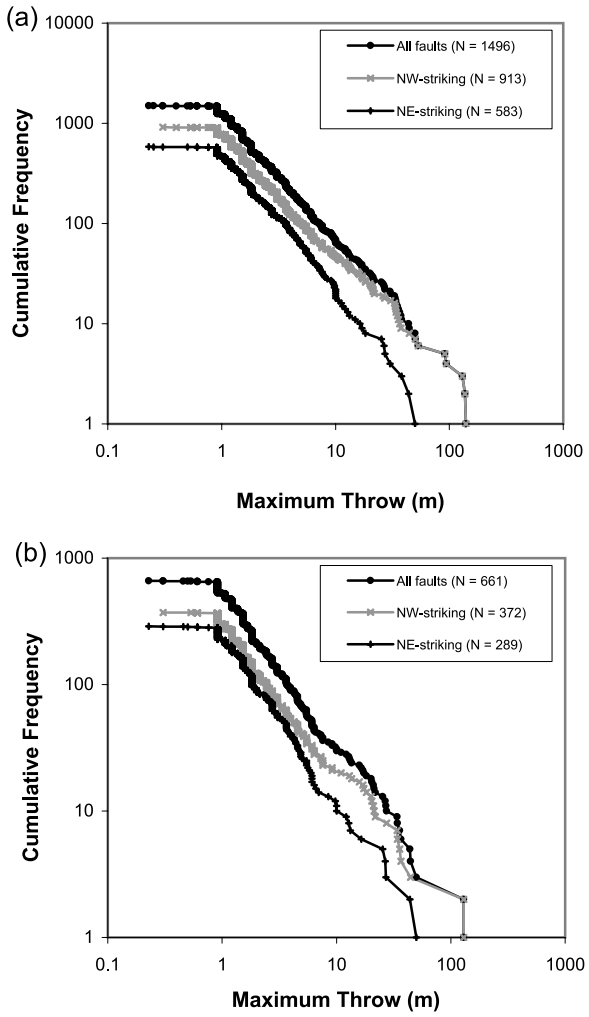

Fig. 9. Maximum throw populations for all faults and for both NW- and NE-striking fault sets from the southern (a) 20×20 km and (b) 10×10 km sub-areas.

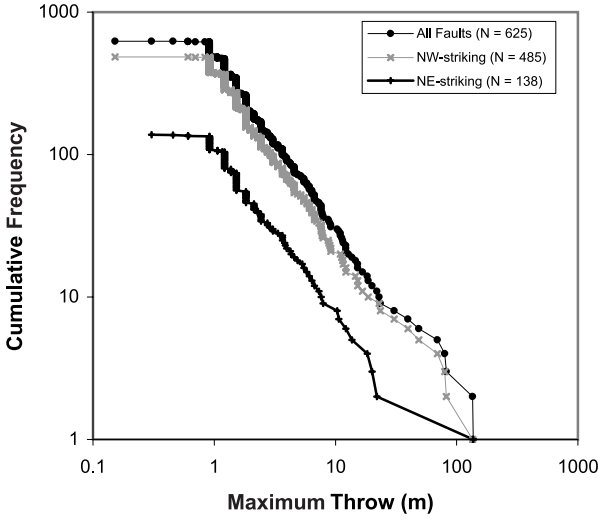

Fig. 10. Maximum throw populations for all faults and for both NW- and NE-striking fault sets from the central 10×10 km sub-area.

6. Discussion

The above data show that the EPC maximum throw population displays a well-defined power-law distribution over two orders of magnitude. Sub-samples of the whole population in 20×20 km and 10×10 km sub-areas also yield power-law distributions with similar population slopes (C_D = 1.19–1.35). Further sub-sampling of the fault population into fault sets with NW- or NE-strikes demonstrates how NW- and NE-striking fault sets contribute differently, in different areas, to regional strain. The regional changes in fault populations are best characterised by the differences in population characteristics in the northern and southern areas (Table 1). In the southern part of the EPC, NW-striking faults are larger, more numerous and accommodate more strain than the NE-striking set and also provide lower slope, and therefore better localised, populations. By contrast, in the northern part of the EPC, NE-striking faults are larger and accommodate more strain than the NW-striking set and provide correspondingly lower population slopes.

We suggest that this regional change in fault geometry and associated fault populations is at least partly attributable to the size, orientation and distribution of the underlying Dinantian structures (Figs. 1 and 2). The significant control of Lower Carboniferous structure on post-Westphalian faulting is supported by evidence from onshore 2-D reflection seismic lines, on which earlier Dinantian faults can often be seen to have been reactivated later and propagated upwards into Westphalian sequences (Fig. 2; see also Fraser and Gawthorpe, 1990). The notion that Dinantian fault architecture has the effect of preferentially localising strain above the largest pre-existing faults is reinforced by visual comparison of the map of major Dinantian faults (Fig. 1b; Fraser and Gawthorpe, 1990) and the EPC coal seam fault map. In the south and central parts of the map, the main faults in the Coal Measures are sub-parallel to and sometimes almost directly overlie the predominantly NW- (WNW–NNW) striking Dinantian faults. The clear spatial association between some post-Westphalian faults and each of the mapped Dinantian faults suggests that reactivation and 3-D linkage is important, though definitive proof of this must await the amalgamation of our coalfield dataset and the seismic datasets from industrial sources. Nevertheless, both fault maps and the locations of the larger (i.e. longer) faults, suggest that approximately NW-striking faults predominate, whilst the NE-striking faults appear to accommodate displacement transfer between the larger NW-striking faults. By contrast, the northern part of the EPC area is polarised in the opposite direction (i.e. the NE striking faults accommodate greater strain), whilst displaying a far more symmetrical fault pattern than that observed in either the southern or the central sub-areas. This northern sub-area straddles the Gainsborough Trough, a Dinantian age half-graben dominated by the ca. 4 km displacement NW-striking Askern–Spital Fault and its lateral equivalent to the NW, the

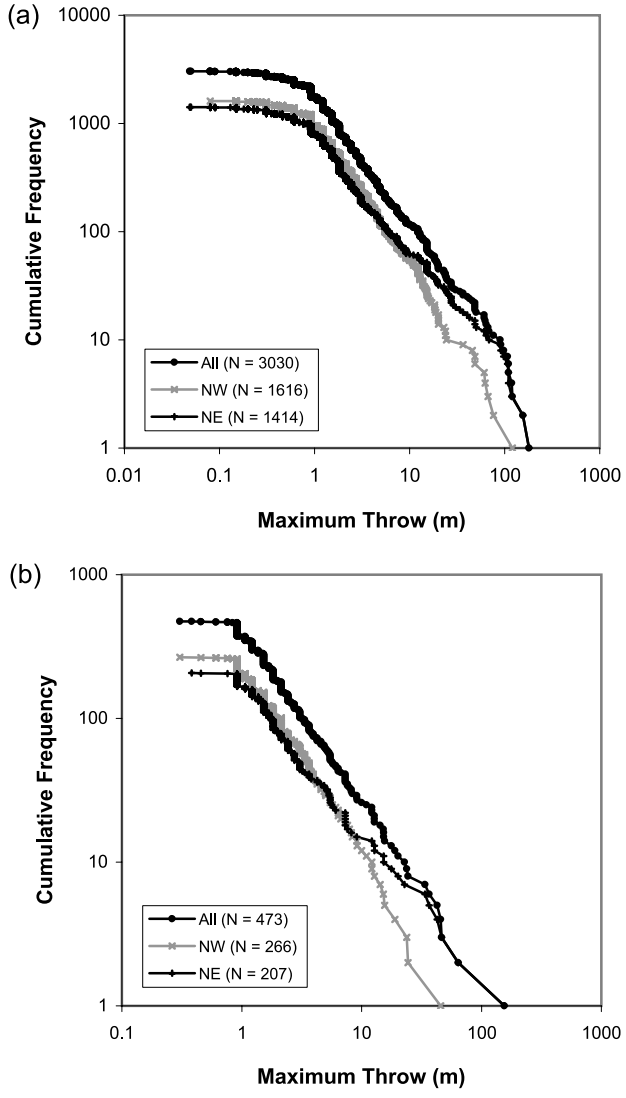

Fig. 11. Maximum throw populations for all faults and for both NW- and NE-striking fault sets from the northern (a) 20×20 km and (b) 10×10 km sub-areas.

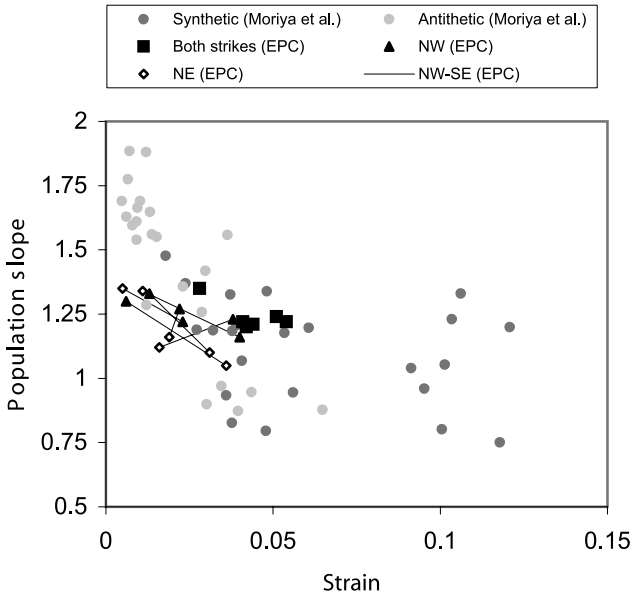

Fig. 12. Strain vs. population slope data for the EPC plotted with synthetic and antithetic fault population data for 11 normal fault systems analysed by Moriya et al. (2005). Since Moriya et al. (2005) used geometric moment/area as their strain measure, this throw-related, rather than heave-related (see Table 1), strain is plotted for the EPC data. Data points for the different fault sets in each EPC sub-area are linked by a line. 'Synthetic' and 'antithetic' refer to the dominant and subordinate dip populations, respectively, studied by Moriya et al. (2005).

Morley–Campsall Fault, which just intersects the NE corner of the northern sub-area (Fig. 1). In the southernmost part of this sub-area, a WNW-striking Dinantian fault appears not to have been reactivated in post-Westphalian times (i.e. it has no clear expression on the EPC map). By contrast, a NE-striking Dinantian fault in the NE is broadly coincident with similarly oriented overlying Westphalian faults and two other NE-striking Dinantian faults occur less than 10 km to the west of this sub-area. The critical difference between this sub-area and those further to the south is the relative paucity of NW-striking Dinantian faults and the appearance of NE striking faults. Acknowledging that the available seismic can only resolve faults with >100 m displacement, we attribute the more symmetrical fault pattern observed in this area (Fig. 4b) to (i) its location above the Gainsborough Trough and the relatively wide spacing (ca. 20 km) between reactivated WNW-striking Dinantian graben-bounding faults and (ii) the presence of NE-striking Dinantian faults. In this setting, the Dinantian faults are reactivated at the margins of the area, but the majority of the fault pattern evolves without an over-riding influence of broadly NW-striking basement faults; instead there is an increased influence from NE-striking structures. The resultant fault pattern displays similarities to those developed in a 3-D stress field with a sub-vertical axis of maximum shortening (Reches, 1978; Krantz, 1988), a pattern which may reflect the original Dinantian fault architecture.

Since the effect of fault reactivation is to preferentially localise displacement on earlier major Dinantian faults, it will have a direct bearing on the nature of fault populations, whatever their orientation. Firstly, higher strain fault sets arising from the reactivation of underlying faults will tend to be better localised and therefore have lower slopes, a characteristic feature of the EPC fault system. Secondly, an increase in localisation through time can lead to the accentuated growth of larger displacement faults with the effect of producing population curves that steepen upwards at progressively smaller displacements (Ackermann and Schlische, 1997; Cowie, 1998; Walsh et al., 2003; Moriya et al., 2005; Fig. 6a). The slight steepening of population curves (i.e. the larger faults (>20 m) are 'over displaced' relative to the smaller (<20 m) faults) for the entire EPC and for the higher strain fault sets of both the northern and southern sub-areas may therefore reflect the preferential localisation of displacement onto larger faults (greater than

ca. 20 m) through time (Figs. 8–11). Another possibility is that sub-sampling could contribute to the generation of upward steepening populations, a suggestion that, in the absence of a well-defined analytical and statistical description of the spatial distributions of this and other fault systems, cannot yet be tested. Finally, fault reactivation and the preferential localisation may also contribute to the apparent upper size limit of EPC faults, an issue that is explored in more detail below.

The possibility that faults within the EPC fault system have an upper size limit (<16 km in length and <180 m maximum throw) is best highlighted by the abrupt tails at the high displacement ends of the maximum throw population curves (Figs. 6a–11). This feature could reflect either a censoring effect or some scale dependent characteristic of the fault system. Censoring is a sampling effect arising from the limited areal extent of a fault map that in this case could be responsible for under-sampling of larger displacement faults which are better represented outside of the EPC area (e.g. Heffer and Bevan, 1990; Pickering et al., 1995). There are two main reasons why this is unlikely to be the case. Firstly, individual sub-areas within the EPC often provide continuous population curves up to ca. 100 m maximum throw and yet the entire EPC population, which is derived from an area that is 4–13 times larger than the sub-areas, does not include larger displacement faults, but instead provides a population curve in which the largest 10 faults are significantly under-displaced. Secondly, there is no evidence from the available seismic data for Westphalian normal fault displacements greater than ca. 200 m, even along the largest Dinantian basin bounding faults of northern England (e.g. Askern–Spittal, Morley–Campsall, Hoton and Wigglesworth Faults; Fraser and Gawthorpe, 1990). We conclude therefore that some other factor controls the upper scale limit. The maximum throw of faults will, to some extent, reflect the maturity of a fault system, such that continued deformation will inevitably increase the maximum throw size. What is surprising, however, is that there are a number of faults with throws similar to this maximum, as well as an upper limit of fault length, which together suggest both immaturity and the presence of a scale-bound characteristic that requires some other explanation. One explanation is that the scaling properties of the faulted sequence may exercise some control on the fault size range. Previous work suggests, for example, that fault scaling could be controlled, to some extent, by the thicknesses and properties of the crust, basin fill or mechanical stratigraphy (e.g. Jackson and White, 1989; Oullion et al., 1996; Gross et al., 1997), in a manner that is analogous to the controls of bedding thickness and rheology on the scaling of layer-bound joint patterns (e.g. Narr and Suppe, 1991; Gross, 1993; Wojtal, 1994, 1996; Gross and Engelder, 1995; Marret, 1996). In that respect the spatial distributions of the largest EPC faults are reminiscent of the relatively regular spatial distributions of joint patterns. There are, however, no grounds for attributing the changes in fault populations across the EPC to equivalent changes in the nature of the faulted sequence. Previous work suggests, in fact, that the mappable inter-coal stratigraphic sequences are usually very heterogeneous at scales below that of the EPC and its sub-areas (Rippon, 1997; Bailey et al., 2002). An alternative explanation is that given that the large-scale geometry of the EPC fault system is to some significant extent inherited from the more mature underlying Dinantian fault system, the characteristic length scales of this system may be comparable with those observed in mature rift systems. Jackson and White (1989) suggested that fault segment lengths of less than ca. 20 km and fault spacings of ca. 20 km are typical of mature rifts and that these limiting scales may be controlled by the elastic thickness of the crust. Since these scaling properties are comparable with those of the EPC (where the largest fault lengths are ca. 16 km and spacing of the largest faults is ca. 20 km), it is possible that the elastic thickness of the crust influenced the size and spacing of major faults during the Dinantian, a structural architecture that is inherited and directly influences the scaling properties of strain in the post-Westphalian fault system. The fact that the Westphalian structure is controlled to some significant extent by earlier Dinantian basin architecture is consistent with, and develops beyond, the arguments presented by Fraser and Gawthorpe (1990), that the structural development of the Dinantian basins are controlled by earlier Caledonian structures, which in the East Pennines is generally NW-striking; west of the Pennines the main Caledonian and Dinantian structural trends swing around the Midland craton to become NE-oriented.

7. Conclusions

Fault population data have been derived from an extremely high-quality fault map (ca. 1300 km^2 area) constructed from mine plans covering the East Pennines Coalfield, central UK. The wide scale range of fault sizes (maximum throw $=0.91$–180 m; lengths ca. 10 m–16 km) contained within the map permits detailed quantitative assessment of the scaling properties of faults and fault-related strain.

2-D fault size (maximum throw and length) populations for the whole EPC provide well-defined power-law distributions. The maximum throw population yields a well-defined power-law exponent of 1.22, but fault length populations are more susceptible to resolution effects, particularly towards fault tips, which result in gently curved distributions. Correcting for this tip resolution effect by adding 60 or 150 m to fault tips produces population curves that approach a power-law distribution with exponents between 1.4 and 1.7. Sub-sets of the entire maximum throw population discriminated in terms of area (20×20 km and 10×10 km sample areas) and strike (NW- and NE-striking fault sets) also define power-law distributions, with slopes

of 1.05–1.35. The differences in population slopes between the different sub-areas and strike sub-sets is a reflection of the strain accommodated by each sub-population, with higher strain populations having more localised deformation, and therefore lower population slopes. In the southern and central parts of the EPC, NW-striking faults dominate the population in terms of size and number, whilst NE-striking faults are more dominant in the north. These differences can be attributed to the influence of the underlying, NW-striking Dinantian faults, above which strain was preferentially localised: the southern and central parts of the EPC sample these structures, whilst the northern area shows an increasing influence from NE-striking Dinantian faults. Size and geometry of the underlying, reactivated Dinanatian fault system is the dominant factor controlling the evolution of the faults in the overlying Upper Carboniferous cover sequence.

Acknowledgements

We thank previous members of the Fault Analysis Group for contributing to the generation of the East Pennines Coalfield Map, including Steve Easton, Marie Eeles, Dan Ellis, Andy Foxford, Paul Gillespie, Nick Lindsay, Dan Sayer and Juan Watterson. Alastair Fraser is thanked for clarification of the details of the fault maps used in Fraser and Gawthorpe (1990). Haakan Fossen and Steve Wojtal are thanked for their constructive reviews.

References

Ackermann, R.V., Schlische, R.W., 1997. Anticlustering of small normal faults around larger faults. Geology 25, 1127–1130.

Ackermann, R.V., Schlische, R.W., Withjack, M.O., 2001. The geometric and statistical evolution of normal fault systems: an experimental study of the effects of mechanical layer thickness on scaling laws. Journal of Structural Geology 23, 1803–1819.

Aitkenhead, N., Chisholm, J.I., Stevenson, I.P., 1985. Geology of the Country Around Buxton, Leek and Bakewell. Memoirs of the British Geological Survey.

Babenroth, J.A., Strahler, A.N., 1945. Geomorphology and structure of the East Kaibab Monocline, Arizona and Utah. Geological Society of America Bulletin 56, 107–150.

Bailey, W.R., Manzocchi, T., Walsh, J.J., Strand, J.A., Nell, P.A., Keogh, K., Hodgetts, D., Flint, S., Rippon, J., 2002. The effects of faults on the 3-D connectivity of reservoir bodies: a case study from the East Pennine Coalfield, UK. Petroleum Geoscience 8, 263–277.

Beck, E., 1929. Salt Creek oil field, Natrona County, Wyoming. In: Structure of Typical American Oilfields II. The American Association of Petroleum Geologists, pp. 589–603.

Bond, D.C., Atherton, E., Bristol, H.M., Buschbach, T.C., Stevenson, D.L., Becker, L.E., Dawson, T.A., Fernalld, E.C., Schawlb, H., Wilson, E.N., Statler, A.T., Stearns, R.G., Buehner, J.H., 1971. Possible future petroleum potential of Region 9—Illinois Basin, Cincinnati Arch and Northern Missippi Embayment. In: Cram, I.H. (Ed.), Future Petroleum Provinces of the United States—their Geology and Potential American Association of Petroleum Geologists Memoir, 1, pp. 1165–1217.

Brunstrom, R.G.W., 1963. Recently discovered oilfields in Britain. In: Proceedings of the 6th World Petroleum Congress, Section 1, Paper 49. Verein zur Forderung, Hamburg, Frankfurt, pp. 11–20.

Cave, R., 1977. Geology of the Malmestry District. Geological Survey of Great Britain.

Cartwright, J.A., Trudgill, B., Mansfield, C.S., 1995. Fault growth by segment linkage: an explanation for scatter in maximum displacement and trace length data from the Canyonlands Grabens of S.E. Utah. Journal of Structural Geology 17, 1319–1326.

Cartwright, J.A., Mansfield, C., Trudgill, B., 1996. The growth of normal faults by segment linkage. In: Buchanan, P.G., Nieuwland, P.G. (Eds.), Modern Developments in Structural Interpretation, Validation and Modelling Special Publication of the Geological Society of London, 99, pp. 163–177.

Childs, C., Walsh, J.J., Watterson, J., 1990. A method for estimation of the density of fault displacements below the limits of seismic resolution in reservoir formations. In: Buller, A.T., Berg, E., Hjelmeland, O., Kleppe, J., Torsæter, O., Aasen, J.O. (Eds.), North Sea Oil and Gas Reservoirs II. Graham and Trotman, London, pp. 309–318.

Cowie, P.A., 1998. A healing-reloading feedback control on the growth rate of seismogenic faults. Journal of Structural Geology 20, 1075–1087.

Cowie, P.A., Scholz, C.H., 1992a. Physical explanation for displacement–length scaling relationship of faults using a post-yield fracture mechanics model. Journal of Structural Geology 14, 1133–1148.

Cowie, P.A., Scholz, C.H., 1992b. Displacement–length scaling relationship for faults: data synthesis and discussion. Journal of Structural Geology 14, 1149–1156.

Cowie, P.A., Sornette, D., Vanneste, C., 1995. Multifractal scaling properties of a growing fault population. Geophysical Journal International 122, 457–469.

Davison, I., 1994. Linked fault systems; extensional, strike-slip and contractional. In: Hancock, P.L. (Ed.), Continental Deformation. Pergamon Press, pp. 121–142.

Dawers, N.H., Anders, M.H., 1995. Displacement–length scaling and fault linkage. Journal of Structural Geology 17, 607–614.

Dawers, N.H., Anders, M.H., Scholz, C.H., 1993. Growth of normal faults: displacement–length scaling. Geology 21, 1107–1110.

Drozdzewski, G., Bournemann, O., Kunz, E., Wrede, V., 1980. Beitraage zur tiefentektonik des Ruhrkarbons. Geologisches Landesmt Nordrhein-Westphalen, Krefeld.

Drozdzewski, G., Engel, H., Wolk, R., Wrede, V., 1985. Beitraage zur tiedentektonik westdeutscher steinkholenlagerstaatten. Geologisches Landesmt Nordrhein-Westphalen, Krefeld.

Elliott, D., 1976. The motion of thrust sheets. Journal of Geophysical Research 81 (5), 949–963.

Elliott, R.E., 1954. Preliminary survey of faults. Internal Report, East Midlands Regional Geological Service, National Coal Board.

Fossen, H., Hesthammer, J., 1998. Deformation bands and their significance in porous sandstone reservoirs. First Break 16, 21–25.

Fox, F.G., 1959. Structure and accumulation of hydrocarbon in southern Foothills, Alberta, Canada. Bulletin of the American Association of Petroleum Geologists 43, 992–1025.

Fraser, A.J., Gawthorpe, R.L., 1990. Tectono-stratigraphic development and hydrocarbon habitat of the Carboniferous in northern England. In: Hardman, R.F.P., Brooks, J. (Eds.), Tectonic Events Responsible for Britain's Oil and Gas Reserves Special Publication of the Geological Society of London, 55, pp. 49–86.

Fraser, A.J., Gawthorpe, R.L., 2003. An atlas of Carboniferous basin evolution in northern England. Geological Society, London, Memoir 28.

Freund, R., 1970. Rotation of strike slip faults in Sistan, southeast Iran. Journal of Geology 78, 188–200.

Frost, D.V., Halliday, D.W., 1980. Geology of the Country around Bellingham. Geological Survey of Great Britain.

Frost, D.V., Smart, J.G.O., 1979. Geology of the Country north of Derby. Geological Survey of Great Britain.

Gauthier, B.D.M., Lake, S.D., 1993. Probabilistic modelling of faults below

the limit of seismic resolution in the Pelican Field, North Sea, offshore U.K.. American Association of Petroleum Geologists Bulletin 77, 761–777.

Gibson, J.R., Walsh, J.J., Watterson, J., 1989. Modeling of bed contours and cross-sections adjacent to planar normal faults. Journal of Structural Geology 11, 317–328.

Gillespie, P.A., 1991. Structural analysis of faults and folds with examples from the South Wales Coalfield and Ruhr Coalfield. Unpublished PhD thesis, University of Wales.

Gillespie, P.A., Walsh, J.J., Watterson, J., 1992. Limitations of dimension and displacement data from single faults and the consequences for data analysis and interpretation. Journal of Structural Geology 14, 1157–1172.

Gillespie, P.A., Howard, C., Walsh, J.J., Watterson, J., 1993. Measurement and characterisation of spatial distributions of fractures. Tectonophysics 226, 113–141.

Goossens, R.F., Smith, E.G., 1973. The stratigraphy and structure of the upper Coal Measures in the Yorkshire coalfield between Pontefract and south Kirkby. Proceedings of the Yorkshire Geological Society 39, 487–514.

Graham, S., 1988. Structural Elements of the Yorkshire Coalfield with Particular Reference to Selby and the Eastern Coal Measures. British Coal, Internal Report.

Gross, M.R., 1993. The origin and spacing of cross-joints: examples from the Monterey Formation, Santa Barbara coastline, California. Journal of Structural Geology 15, 737–751.

Gross, M.R., Engelder, T., 1995. Strain accommodated by brittle failure in adjacent units of the Monterey Formation, U.S.A.: scale effects and evidence for uniform displacement boundary conditions. Journal of Structural Geology 17, 1303–1318.

Gross, M.R., Gutiérrez-Alonso, G., Bai, T., Wacker, M.A., Collinsworth, K.B., 1997. Influence of mechanical stratigraphy and kinematics on fault scaling relations. Journal of Structural Geology 19, 171–183.

Heffer, K.J., Bevan, T.G., 1990. Scaling relationships in natural fractures. Journal of Structural Geology 13, 735–738.

Huntoon, P.W., 1974. The post-Palaeozoic structural geology of the Eastern Grand Canyon, Arizona. In: Geology of the Grand Canyon. Museum of Northern Arizona and Grand Canyon Natural History Association, Arizona, pp. 82–115.

Jackson, J.A., White, N.J., 1989. Normal faulting in the upper continental crust: observations from regions of active extension. Journal of Structural Geology 11, 15–36.

Jackson, J., Norris, R., Youngson, J., 1996. The structural evolution of active fault and fold systems in central Otago, New Zealand: evidence revealed by drainage patterns. Journal of Structural Geology 18 (2/3), 217–234.

Jackson, P., Sanderson, D.J., 1992. Scaling of fault displacements from the Badajoz–Cordobe shear zone, SW Spain. Tectonophysics 210, 179–190.

Janoschek, R.H., Götzinger, K.G.H., 1969. Exploration for oil and gas in Austria. In: Hepple, P. (Ed.), The Exploration for Petroleum in Europe and North Africa. Elsevier, London, pp. 161–180.

Kakimi, T., 1980. Magnitude–frequency relation for displacement of minor faults and its significance in crustal deformation. Bulletin of the Geological Society of Japan 31, 467–487.

Krantz, R.W., 1988. Multiple fault sets and three-dimensional strain: theory and application. Journal of Structural Geology 10, 225–237.

MacMillan, R.A., 1975. The orientation and sense of displacement of strike-slip faults in continental crust. Unpublished B.S. thesis, Carelton University, Ottawa, Ontario.

Marret, R., 1996. Aggregate properties of fault populations. Journal of Structural Geology 18, 169–178.

Marret, R., Allmendinger, R.W., 1990. Kinematic analysis of fault-slip data. Journal of Structural Geology 12, 973–986.

Marret, R., Allmendinger, R.W., 1991. Estimation of strain due to brittle faulting: sampling of fault populations. Journal of Structural Geology 12, 973–986.

Marret, R., Allmendinger, R.W., 1992. Amount of extension on "small" faults: an example from the Viking Graben. Geology 20, 47–50.

Mayuga, M.N., 1970. Geology and development of California's Giant–Wilmington Oil Field. In: Halbouty, M.T. (Ed.), Geology of Giant Petroleum Fields American Association of Petroleum Geologists, Memoir, 14, pp. 158–184.

MFRG (Minor Faults Research Group), 1973. A minor fault system around the Otaki area, Boso Peninsula, Japan. Earth Science (Chikyu Kagaku) 27, 180–187.

Moriya, S., Childs, C., Manzocchi, T.M., Walsh, J.J., 2005. Analysis of the relationships between strain, polarity and population slope for normal fault systems. Journal of Structural Geology, in press.

Muraoka, H., Kamata, H., 1983. Displacement distribution along normal fault traces. Journal of Structural Geology 5, 483–495.

Narr, W., Suppe, J., 1991. Joint spacing in sedimentary rocks. Journal of Structural Geology 13, 1037–1048.

Nelson, P.H.H., 1980. Role of reflection seismic in development of Nembe Creek Field, Nigeria. In: Halbouty, M.T. (Ed.), Giant Oil and Gas Fields of the Decade: 1968–1978 American Association of Petroleum Geologists, 30, pp. 565–576.

Nicol, A., Watterson, J., Walsh, J.J., Childs, C., 1996. The shapes, major axis orientations and displacement patterns of fault surfaces. Journal of Structural Geology 18, 235–248.

Opheim, J.A., Gudmundsson, A., 1989. Formation and geometry of fractures, and related volcanism, of the Krafla fissure Swarm, northeast Iceland. Geological Society of America Bulletin 101, 1608–1622.

Oullion, G., Castaing, C., Sournette, D., 1996. Hierarchical geometry of faulting. Journal of Geophysical Research 101B, 5477–5487.

Peacock, D.C.P., 1991. Displacements and segment linkage in strike-slip fault zones. Journal of Structural Geology 13, 1025–1035.

Pickering, G., Bull, J.M., Sanderson, D.J., Harrison, P.V., 1994. Fractal fault displacements. A case study from the Moray Firth, Scotland. In: Kruhl, J.H. (Ed.), Fractals and Dynamic Systems in Geosciences. Springer-Verlag, Berlin, pp. 105–120.

Pickering, G., Bull, J.M., Sanderson, D.J., 1995. Sampling power-law distributions. Tectonophysics 248, 1–20.

Poulimenos, G., 2000. Scaling properties of normal fault populations in the western Corinth Graben, Greece: implications for fault growth in large strain settings. Journal of Structural Geology 22, 307–322.

Ranalli, G., 1977. Correlation between length and offset in strike-slip faults. Tectonophysics 37, T1–T7.

Reches, Z., 1978. Analysis of faulting in three-dimensional strain field. Tectonophysics 47, 109–129.

Reeves, J.R., 1929. El Dorado Oil Field, Butler County, Kansas. American Association of Petroleum Geologists.

Rippon, J.H., 1985a. Contoured patterns of the throw and hade of normal faults in the Coal Measures (Westphalian) of north-east Derbyshire. Proceedings of the Yorkshire Geological Society 45, 147–161.

Rippon, J.H., 1985b. New methods of forecasting the throw and hade of faults in some North Derbyshire Collieries. Transactions of the Institute of Mining Engineers 145, 198–204.

Rippon, J.H., 1997. Variations in tectonic style and setting in British coalfields. Unpublished PhD thesis, University of Keele, UK.

Rowan, M.G., 1997. Three-dimensional geometry and evolution of a segmented detachment fold, Mississippi fan foldbelt, Gulf of Mexico. Journal of Structural Geology 19 (3-4), 463–480.

Ruzhich, V.V., 1977. Relations between fault parameters and practical application of them. In: Mekhanizmy Structur Vostochronochnoisibiri Novisbirsk (in Russian).

Schlische, R.W., Young, S.S., Ackermann, R.V., Gupta, A., 1996. Geometry and scaling relations of a population of very small rift-related normal faults. Geology 24, 683–686.

Scholz, C.H., Cowie, P.A., 1990. Determination of total strain from faulting using slip measurements. Nature 346, 837–838.

Scholz, C.H., Dawers, N.H., Yu, J.-J., Anders, M.A., Cowie, P.A., 1993. Fault growth and scaling laws: preliminary results. Journal of Geophysical Research 85, 21,951–21,961.

Schultz, R.A., Fossen, H., 2002. Displacement–length scaling in three-dimensions: the importance of aspect ratio and application to deformation bands. Journal of Structural Geology 24, 1389–1411.

Shepherd, J., Burns, K.L., 1978. Fault swarms in the Greta Coal Seam, New South Wales. Proceedings of the Australasian Institute of Mining and Metallurgy 267, 27–36.

Teas, L.P., 1929. Irma oil field, Nevada County, Arkansas. In: Structure of Typical American Oilfields: American Association of Petroleum Geologists Annual Symposium 1. American Association of Petroleum Geologists, Tulsa, pp. 1–17.

Tschop, R.H., 1967. Development of the Fahud Field. In: 7th World Petroleum Congress. Elsevier, London, Mexico, pp. 243–250.

Van den Bark, E., Thomas, O.D., 1981. Ekofisk: first of the giant oil fields in Western Europe. American Association of Petroleum Geologists Bulletin 65 (11), 2341–2363.

Verdier, A.C., Oki, A.C., Suardy, A., 1980. Geology of the Handil Field (East Kalimanton–Indonesia). In: Halbouty, M.T. (Ed.), Giant Oil and Gas Fields of the Decade: 1968–1978 Association of Petroleum Geologists Memoir, 30, pp. 399–421.

Villemin, T., Sunwoo, C., 1987. Distribution logarithmique self similaire des rejets et longeurs de failles: exemple du basin Houllier Lorrain. Comptes Rendus de l'Académie des Sciences 305 (II), 1309–1312.

Villemin, T., Angelier, J., Sunwoo, C., 1995. Fractal distribution of fault length and offsets: implications of brittle deformation evaluation—Lorraine Coal Basin. In: Barton, C.C., La Pointe, P.R. (Eds.), Fractals in the Earth Sciences. Plenum Press, New York, pp. 205–226.

Walsh, J.J., Watterson, J., 1988a. Dips of normal faults in British Coal Measures and other sedimentary sequences. Journal of the Geological Society of London 145, 859–873.

Walsh, J.J., Watterson, J., 1988b. Analysis of the relationship between the displacements and dimensions of faults. Journal of Structural Geology 10, 239–247.

Walsh, J.J., Watterson, J., 1989. Displacement gradients on fault surfaces. Journal of Structural Geology 11, 307–316.

Walsh, J.J., Watterson, J., 1990. New methods of fault projection for coalmine planning. Proceedings of the Yorkshire Geological Society 48, 209–219.

Walsh, J.J., Watterson, J., 1991. Geometric and kinematic coherence and scale effects in normal fault systems. In: Roberts, A.M., Yielding, G., Freeman, B. (Eds.), The Geometry of Normal Faults Special Publication of the Geological Society of London, 56, pp. 193–203.

Walsh, J.J., Nicol, A., Childs, C., 2002. An alternative model for the growth of faults. Journal of Structural Geology 24, 1669–1675.

Walsh, J.J., Childs, C., Imber, J., Manzocchi, T., Watterson, J., Nell, P.A.R., 2003. Strain localisation and population changes during fault system growth within the Inner Moray Firth, Northern North Sea. Journal of Structural Geology 25, 307–315.

Watterson, J., 1986. Fault dimensions, displacements and growth. Pure and Applied Geophysics 124, 365–373.

Watterson, J., Walsh, J.J., Gillespie, P.A., Easton, S., 1996. Scaling systematics of fault sizes on a large scale range fault map. Journal of Structural Geology 18, 199–214.

Wojtal, S.F., 1994. Fault scaling laws and temporal evolution of fault systems. Journal of Structural Geology 16, 603–612.

Wojtal, S.F., 1996. Changes in fault displacement populations correlated to linkage between faults. Journal of Structural Geology 18, 265–280.

Wood, G.H., Trexler, J.P., Kehn, T.M., 1969. Geology of the west-central part of the Southern Anthracite field and adjoining areas, Pennsylvania. Geology Survey, Professional paper.

Woodcock, N.H., Strachan, R.A., 2000. Geological History of Britain and Ireland. Blackwell Science.

Woodland, A.W., Evans, W.B., 1964. The Geology of the South Wales Coalfield. Part IV. The Country around Pontypridd and Maesteg. H.M.S.O., London.

Yielding, G., Needham, D.T., Jones, H., 1996. Sampling of fault populations using sub-surface data: a review. Journal of Structural Geology 18, 135–146.